Energy bands and Fermi surface of Sr_2RuO_4

Canio Noce and Mario Cuoco
Unità INFM di Salerno, Dipartimento di Scienze Fisiche ''E.R. Caianiello,'' Università di Salerno, I-84081 Baronissi (Salerno), Italy
(Received 26 January 1998; revised manuscript received 15 May 1998)

A method combining the extended Hückel theory and the tight-binding approximation is proposed to study the electronic properties of the layered noncuprate superconductor Sr_2RuO_4. The band structure close to the Fermi level is obtained by integrating out all low-lying oxygen degrees of freedom allowing the determination of the energy spectra, the Fermi surface, and the total density of states. The results reproduces the main features of local-density approximation calculations near the Fermi energy. As an application of the approach here proposed, we have calculated the temperature dependence of the in-plane Hall coefficient considering the effect of the curvature of the Fermi surface. [S0163-1829(99)11903-9]

I. INTRODUCTION

One of the common features in cuprate high-T_c superconducting oxides (HTS) is that all of them have a layered perovskite structure with CuO_2 conducting planes. In spite of great efforts, noncuprate superconducting oxides with layered perovskite structure have not been found until recently. The discovery of superconductivity at $T_c \sim 1$ K in noncuprate compound Sr_2RuO_4 by Maeno *et al.*,[1] has generated a lot of interest in this material chiefly because of its similarities to HTS. It has crystal structure similar to the cuprate superconductor $(La,Sr)_2CuO_4$, it is near a magnetic instability and it was thought to be (quite) strongly correlated. However, a closer inspection reveals some differences from cuprates. Among the differences we mention: the density of states at the Fermi level E_F is about twice that of HTS; the antibonding orbitals at E_F are derived from d_{xy}, d_{xz}, and d_{yz} orbital combinations rather than the $d_{x^2-y^2}$ orbital as in HTS; there are three sheets forming the Fermi surface (FS) rather than one as in HTS; the critical temperature is two orders of magnitude smaller than in HTS and it is superconductor without doping. Finally, it has been recently suggested that the superconductivity in Sr_2RuO_4 could be of *p*-wave type[2–4] and thus very different from the HTS cuprates.

Band structure calculations independently carried out by Oguchi,[5] Singh,[6] and MacMullan, Ray, and Needs[7] show the coexistence of three partially filled two dimensional bands: one hole type and two electron type. Mackenzie *et al.*[8] and Yoshida *et al.* [9] have confirmed the image of the one hole and two electron bands observing three fundamental frequencies in de Haas–van Alphen (dHvA) oscillations. In particular, the FS consists of three corrugated cylinders and corresponds to four electrons in the Brillouin zone according to the prediction of Luttinger's theorem that the Fermi volume is conserved even in presence of strong electron interactions.

Nevertheless it seems that there is disagreement between dHvA results and angle-resolved photoemission spectroscopy (ARPES) measurements.[10] Indeed ARPES studies of Sr_2RuO_4 show a FS consisting of two small hole sheets and one electronlike Fermi surface.

Concerning the low-temperature transport properties, some interesting results have recently been obtained. The Hall coefficient exhibits a complicated temperature behavior:[11] it is negative at very low temperatures, it changes sign at temperatures approximately above 30 K and shows a return to negative values above approximately 130 K. As far as resistivity is concerned,[12,13] in contrast with the metallic in-plane resistivity ρ_{ab}, the out-of-plane resistivity ρ_c takes a maximum at about 130 K and changes to nonmetallic temperature dependence at higher temperatures. Therefore $3d$-$2d$ crossover of metallic conduction occurs. Below approximately 25 K both ρ_{ab} and ρ_c exhibit a T^2 power-law behavior quite accurately. The *c*-axis magnetoresistance[13] is large and positive and varies linearly with the applied magnetic field; with the increase of temperature it falls sharply becoming negative above 75 K. The in-plane magnetoresistance is positive and large at low temperatures, then decreases as T is raised up to 80 K. For other electronic transport properties, the Seebeck coefficient has been reported by Yoshino *et al.*[14] and the electronic Raman scattering by Yamanaka *et al.*[15]

The integrated ultraviolet photoemission spectra by Inoue *et al.*[16] reveal states reminiscent of the lower Hubbard band. An on-site Coulomb repulsion of 2.4 eV is estimated from the spectra and in conjunction with the one-particle bandwidth of 1.4 eV gives a ratio of $U/W = 1.7$, which indicates that Sr_2RuO_4 is a less strongly correlated system compared to HTS. This implies that the band structure of Sr_2RuO_4 as obtained from local-density approximation (LDA) calculations as well as from the tight-binding approach, where correlation effects are neglected, gives some insights on the effective band spectra of the ruthenate superconductor.

In this paper we calculate the electronic band structure and the FS of Sr_2RuO_4 using a method that combines the extended Hückel approximation and the tight-binding approach. It is worth stressing that even if LDA calculations are available, they are rather complicated and are not delivered in a form useful as the single-particle term of a correlated model Hamiltonian that describes the low-energy excitations. As a result, for instance for HTS, most theorists neglect the LDA band structure, or at least its nontrivial details, and use the simplest possible Cu-Cu one-band two-center orthogonal tight-binding model with hopping integrals between only nearest and next-nearest neighbors.[17]

Based on the analysis of the LDA bands for Sr_2RuO_4, we

 ©1999 The American Physical Society

derive a simple tight-binding model with an analytical expression for band dispersion near E_F together with the determination of FS. This result turns out to be readily used in calculating physical quantities dependent on the explicit form of the energy spectrum as well as on the real shape of FS. As an example, and for realistic temperature law for the relaxation rate, we have computed the in-plane Hall coefficient.

Besides, it is our hope that the model will be used in the future for the single-particle term in more sophisticated Hamiltonians containing for instance Coulomb correlations as well as the Hund coupling.[18]

We notice that some preliminary results on this type of calculation have already been presented.[19] Nevertheless, it is worth stressing that in that paper a two-dimensional analysis of electronic spectra has been considered, neglecting the k_z dispersion of the bands and putting the bare energy ordering of d orbitals by hand in order to fit the LDA curves, without any physical motivation. Indeed, the energy of d_{xz} and d_{yz} Ru orbitals was assumed to be the same and, according to linear muffin tin calculations,[7] the energy of d_{xy} orbital was supposed lower than the energy of the other d orbitals.

The combined extended Hückel theory–tight-binding method here presented overcomes this difficulty: the extended Hückel approach gives information about the ordering in energy of the molecular orbitals and their composition and thus the tight-binding calculation allows us the explicit determination of energy spectra as well as the FS. From the composition of molecular orbitals we also obtain the overlap between the orbitals belonging to different atoms and this in turn gives some information on the strength of hopping terms in the tight-binding Hamiltonian.

The paper is organized as follows: in the next section the method employed to calculate the energy bands and FS is presented while in Sec. III it is applied to Sr_2RuO_4 and the results are discussed. Section IV is devoted to the conclusions.

II. METHOD OF CALCULATION

The crystal structure of Sr_2RuO_4 is the body-centered tetragonal K_2NiF_4 type with the $I4/mmm$ space group. The Ru atom and the two plane O [O(1)] atoms are coplanar and form a two-dimensional square lattice. The Ru atom is coordinated above and below by the apical O(2) atoms in the double SrO rocksalt layers. The Sr atoms lie above and below the hollow spaces in the centers of squares formed by Ru atoms. The fractional atomic coordinates are given by Sr $[0,0,z(\mathrm{Sr})]$; Ru (0,0,1/2); O(1) (0,1/2,0); O(2) $[0,0,z(\mathrm{O})]$ and the lattice constants and the parameters are $a=3.8603$ Å, $c=12.729$ Å, $z(\mathrm{Sr})=0.3524(3)$ and $z(\mathrm{O})=0.1635(3)$, at $T=100$ K.[20]

The in-plane Ru-O(1) distance is 1.9301 Å which is less than the sum of Ru^{4+} and O^{2-} ionic radii, suggesting the possibility of significant hybridization between these two atoms, whereas the apical oxygen O(2) height is 2.06 Å, i.e., larger than the sum of ionic radii.

The present energy band calculation is performed in two steps. First we apply the extended Hückel theory (EHT) to Sr_2RuO_4 determining the energy of molecular orbitals (MO's) and their composition, and then we introduce a tight-binding model for the ruthenate superconductor.

Let us now briefly summarize the EHT. The starting point is the local combination of atomic orbitals expansion:

$$\psi=\sum_n c_n\varphi_n . \tag{1}$$

The task is to find the coefficient $\{c_n\}$ in Eq. (1), $\{\varphi_n\}$ being the atomic orbitals. The substitution of Eq. (1) into the Schrödinger equation $H\psi=E\psi$ leads to

$$\sum_n c_n(H-E)\varphi_n=0 \tag{2}$$

and, if we multiply this equation by each of the basis function φ_n on turn and integrate, we obtain the secular equation, one for each value of m:

$$\sum_n c_n(H_{mn}-ES_{mn})=0. \tag{3}$$

Here $H_{mn}=\int\varphi_m^* H\varphi_n dV$ and $S_{mn}=\int\varphi_m^*\varphi_n dV$.

The energies of the orbitals are obtained by equating the secular determinant to zero and each value of E that is a solution to this equation can be substituted back into Eq. (2) to obtain the coefficients $\{c_n\}$, apart from a normalizing factor. In standard Hückel theory, all the nondiagonal overlap integrals S_{mn} are assumed to be zero whereas the off-diagonal integrals H_{mn}, the so-called resonance integrals, are equal to a constant β and H_{nn}, the Coulomb integrals, are written as constant α. In EHT the Coulomb integrals are given fixed values that have been assigned using spectroscopic data. The resonance integrals are calculated from the following formula:

$$\beta_{nm}=\frac{k}{2}(\alpha_n+\alpha_m)S_{nm}, \tag{4}$$

where k is an adjustable parameter taken for instance in the Hoffmann approach[21] to have the value 1.75 and $\alpha_n=H_{nn}$.

The overlap integrals S_{nm} are calculated and included in the secular Eq. (3) so that all S_{nm} and hence β_{nm} both between orbitals on neighboring atoms and between orbitals on non-neighboring atoms, are included in the calculation. The calculation can be carried out for a fixed geometry or the geometry can be varied to determine the molecular configuration with the minimum energy. It is worth mentioning that EHT has been recently used to analyze the electronic structure of two families of HTS superconductors, namely $TlBa_2Ca_{n-1}Cu_nO_{2n+3}$ and $Tl_2Ba_2Ca_{n-1}Cu_nO_{2n+4}$ for $n=1,2,3,4$.[22]

Using the crystal parameters previously reported we have applied EHT to Sr_2RuO_4. The results are summarized in Table I, where only the MO with energy near to E_F are reported. In the table are indicated, for each MO (column 1), the corresponding energy (column 2), the atomic orbitals involved (column 3), the corresponding composition in percentage (column 4) and finally the phase factors of the atomic orbitals (column 5). The oxygen atoms (O1[{a,0,0}],O2[{0,a,0}]) and (O3[{0,0,c}], O4[{0,0,$-c$}]) denote the planar and the apical ones, respectively. From the data reported in this table some consid-

TABLE I. EHT results for MO near the Fermi level. In the first column is reported the number of the corresponding MO; in the second colunm is reported the corresponding energy value; column 3 contains the atomic orbitals contributing the to MO, together with the percentage (column 4) and the phase factor (column 5). O1 and O2 denote the oxygen orbitals along *a* and *b* axis, respectively; O3 and O4 indicates the apical oxygen orbitals above the *a*-*b* plane and below it, respectively. The energies of MO are measured with respect to MO 3.

MO	Energy (eV)	Orbitals	%	Phase factor
1	0.55	Ru d_{xz}	42	+
		Ru d_{yz}	42	−
		O1 p_z	4	−
		O2 p_z	4	+
		O3 p_x	2	−
		O3 p_y	2	+
		O4 p_x	2	+
		O4 p_y	2	+
2	0.55	Ru d_{xz}	42	+
		Ru d_{yz}	42	+
		O1 p_z	4	−
		O2 p_z	4	−
		O3 p_x	2	−
		O3 p_y	2	−
		O4 p_x	2	+
		O4 p_y	2	+
3	0	Ru d_{xy}	84	+
		O1 p_y	8	−
		O2 p_x	8	−

erations are in order. All the orbitals have predominantly Ru $4d$ character, with an orbital composition of 84% Ru $4d$ and 16% O $2p$. This result agrees quite well with the near-edge x-ray-absorption and valence-band photoemission spectroscopy experimental data[23] that estimate the orbital contribution at E_F as 80% Ru $4d$ and 20% O $2p$. For completeness we mention that HTS exhibit a composition of orbitals as 20% Cu and 80% O $2p$ at E_F. The MO 3 is planar in the sense that it is composed by orbitals that lie in the *a*-*b* plane and the orbitals entering its composition decouple completely from Ru $4d$ and O $2p$ orbitals that give rise to MO 1 and 2. Finally we notice that from EHT analysis we find that the MO 3 has the lowest energy compared to MO 1 and 2 that are degenerate.

In a tetragonal complex the *d* orbitals divide into two sets due to the ligand field splitting. The two e_g orbitals lie above the three t_{2g} orbitals; the t_{2g} orbitals also split into two sets with d_{xz}, d_{yz} orbitals below the d_{xy} orbital. Thus, as a consequence of the crystal-field theory (CFT), the energies of t_{2g} *d* orbitals lie in the order $d_{xz}=d_{yz}<d_{xy}$. Nevertheless in this approach the complex is modeled as a central ion surrounded by ligands that act only as a source of electric potential. In other words, they are not regarded as supplying atomic orbitals from which molecular orbitals spreading over the entire complex may be formed. The ligands produce a potential that removes the degeneracy of the orbitals of the central ion, and the structure of the complex can be discussed in terms of the building-up principle applied to the set of

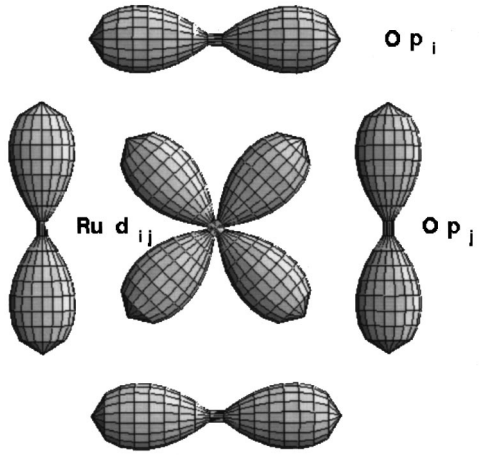

FIG. 1. Orbitals producing the hybridized bands. The central *d* orbital corresponds to one of the t_{2g} orbitals while the surrounding ones are the *p* orbitals. The following notation is adopted: d_{ij} denotes one of the d_ϵ orbitals, $ij=\{(xy),(xz),(yz)\}$, and p_i, p_j refer to oxygen orbitals.

energy levels produced in this way. We have to observe that the planar oxygen, as in the layered cuprates, has significant open shell character so that the ionic picture is only approximately correct; this implies that the results obtained in accordance with CFT cannot be considered satisfactory when the bond between the central atom and the ligands is far from being ionic. The strictest approach to the problem of the nature of the bond in complex compounds is to use the method of molecular orbitals, although this involves much greater difficulties than the crystal-field approach. The EHT, taking into account the overlap integrals S_{nm} as well as the resonance integrals, gives a result more accurate than the one derived from the CFT. The result we obtain agrees with the LDA conclusion that at Γ point the band originating from d_{xy} orbital is lower in energy than the other two bands, and this in turn implies that the bare d_{xy} energy can be assumed smaller than the bare d_{xz}-d_{yz} energy.

Let us now introduce a tight-binding model for Sr_2RuO_4.

The relevant orbitals producing the hybridized *d*-bands are reported in Fig. 1. We adopt for the phase factors the standard convention, i.e., the lobes of the orbitals have $+/-$ according to the sign of the corresponding wave function.

A. d_{xy} band

Taking advantage of EHT results we assume that this band contains only Ru d_{xy} and O1 $2p_y$ and O2 $2p_x$ orbitals along *a* and *b* axes, respectively. If we assume that only the nonzero hopping integrals between neighboring Ru and O orbitals and those between two neighboring O are important, it is straightforward to show that the low-energy excitation of electrons is described by the following tight-binding Hamiltonian:

$$H_{xy}=\sum_k D^\dagger \begin{pmatrix} \epsilon_{xy} & it_{1x}(k) & it_{1y}(k) \\ -it_{1x}(k) & \epsilon_p & t_2(k) \\ -it_{1y}(k) & t_2(k) & \epsilon_p \end{pmatrix} D, \quad (5)$$

where $D^\dagger=(d^\dagger_{xy},p^\dagger_{1y},p^\dagger_{2x})$ are the electron creation operators in the k space corresponding to the above three orbitals, specifically, $p^\dagger_{1y}$ ($p^\dagger_{2x}$) refers to the creation of electrons on $2p_y$ ($2p_x$) orbital located at O1 (O2) and $d^\dagger_{xy}$ creates electrons on d_{xy} orbital; ϵ_{xy} and ϵ_p are the energy of d_{xy} and p states, respectively. The off-diagonal matrix elements in H_{xy} are $t_{1i}(k)=-2t_{1i}\sin(k_i/2)$ $(i=x,y)$ and $t_2(k)=-4t_2\sin(k_x/2)\sin(k_y/2)$, where t_{1i} is the hopping integral between d_{xy} and p_i states ($p_1=p_{1y}$, $p_2=p_{2x}$) and t_2 is the hopping integral between p_{1y} and p_{2x} states.

B. d_z bands

The orbitals contributing to these bands are the d_{xz}, d_{yz}, and $2p_z$ belonging to the Ru and O atoms in the plane, respectively, and the $2p_{x,y}$ of the O atoms out of plane. As for xy band, we assume only the hopping integrals between Ru and O orbitals and those between two neighboring O are nonvanishing. Under these assumptions the tight-binding Hamiltonian is

$$H_z=\sum_k C^\dagger \begin{pmatrix} \epsilon_d & 0 & -ie_k & 0 & -ig_k & 0 \\ 0 & \epsilon_d & 0 & -if_k & 0 & -ig_k \\ ie_k & 0 & \epsilon_p & a_k & -ib_k & 0 \\ 0 & if_k & a_k & \epsilon_p & 0 & -ic_k \\ ig_k & 0 & ib_k & 0 & \epsilon_p & 0 \\ 0 & ig_k & 0 & ic_k & 0 & \epsilon_p \end{pmatrix} C, \tag{6}$$

where $C^\dagger=(d^\dagger_{xz},d^\dagger_{yz},p^\dagger_{1z},p^\dagger_{2z},p^\dagger_{3x},p^\dagger_{3y})$ are the creation operators in the k space corresponding to the above six orbitals. In particular, $p^\dagger_{1z}$ ($p^\dagger_{2z}$) denotes the creation operator of electrons on $2p_z$ orbital along a (b) axis and $p^\dagger_{3x}$ ($p^\dagger_{3y}$) refers to the creation operator of electrons on apical $2p_x$ ($2p_y$) orbital at the O3 site. ϵ_d and ϵ_p are the energies of d_{xz}, d_{yz}, and $p_{x,y,z}$ states, respectively. The off-diagonal elements of H_z are: $a_k=-4t_3\cos(k_x/2)\cos(k_y/2)$; $b_k=4t_4\cos(k_x/2)\sin(k_z/2)$; $c_k=4t_4\cos(k_y/2)\sin(\alpha k_z/2)$; $e_k=2t_5\sin(k_x/2)$; $f_k=2t_5\sin(k_y/2)$; $g_k=2t_6\sin(\alpha k_z/2)$. Here t_3 is the hopping integral between two O p_z planar orbitals; t_4 is the hopping integral between apical O $p_{3x,y}$ and planar O $p_{1,2z}$; t_5 (t_6) is the hopping integral between d_{xz}, d_{yz}, and $p_{1,2z}$ ($p_{3x,y}$) states and finally α is the ratio of the distances Ru-O1 and Ru-O3.

As previously pointed out there are three bands crossing E_F. The energy dispersion of these three bands can be obtained by integrating out all low-lying O $2p$ degrees of freedom using the Löwdin down-folding procedure.[24] The energy-band dispersions we obtain are $E_{1,2,3}(k)$, where $E_{1,2}(k)$ and $E_3(k)$ denote the bands derived from a combination of Ru d_{xz}, d_{yz} and from Ru d_{xy} orbitals, respectively. The explicit expression of these energies are reported in the Appendix.

III. RESULTS AND DISCUSSION

We fix the parameters in H_{xy} and H_z by requiring that the volumes enclosed by the three bands coincide with those measured in quantum oscillations, i.e., 0.475 and 0.667 for the electron bands (E_2 and E_3, respectively) and 0.108 for the hole band (E_1) and the composition of MO is the same as deduced from EHT, i.e., the relative values of the strength of hopping parameters are fixed by the composition of MO. Besides, the LDA result $\epsilon_d-\epsilon_p=1.5$ eV is used to fix the overall energy scale. The parameters we obtained with the above fitting procedure are $(t_1,t_2,t_3,t_4,t_5,t_6)=(1.1,-0.52,0.1,0.025,0.85,0.25)$ eV and $(\epsilon_p,\epsilon_{xy},\epsilon_d)=(-2.4,-1.9,-0.9)$ eV.

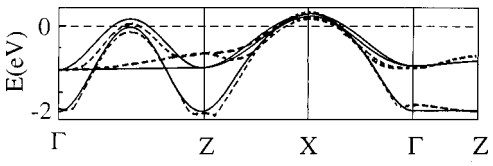

FIG. 2. Calculated energy band structure along high-symmetry lines (thin lines), near the Fermi level (dashed line). The energy band structure calculated within the LDA method by Singh (Ref. 6) is also presented (dashed lines). In this latter case only the bands close to E_F are reported.

Figure 2 shows the energy dispersion (thin lines) for the above three bands along a few high-symmetry lines. The bands structure near and below E_F is strongly anisotropic and all the bands show a very little dispersion along the k_z axis, as is evident from the small dispersion along the short Γ-Z direction. It is worth mentioning that $E_3(k)$ is k_z dispersionless by construction.

We want to stress that our simple calculations reproduce the main features of LDA band structure, i.e., $E_{1,2}(k)$ bands are degenerate at Γ point, the band maxima locate at X point for all three bands and $E_3(k)$ is more dispersive. This is evident from the same Fig. 2 where the band structure near E_F obtained by Singh[6] is reported (thick lines). The agreement between LDA computations and our calculations gives confidence that our simplified model captures the essential physics of Sr_2RuO_4 at least near E_F.

Fermi surface is shown in Fig. 3. It consists of three almost cylindrical sheets: two of such sheets are large electronlike cylinders centered at Γ point and the last surface is hole-like cylinder centered at X point. In particular, the surface associated with the Ru d_{xy} state forms a cylindrical sheet showing no dispersion along the k_z direction while the other two bands give rise to corrugated cylinders. It is worth noticing that very recent angular dependent dHvA oscillations experiments[9] show three almost cylindrical branches, but little corrugated. In our calculations the bands originating from Ru d_{xz}-d_{yz} agree in the shape with the experimental results, but that produced by Ru d_{xy} shows no modulation along the k_z axis for symmetry reasons. Of course a more detailed analysis needs to explain the experimental data. For instance, exchange terms between electrons in the t_{2g} Ru d orbitals connecting in an indirect way the d_{xy} orbital to apical oxygen orbitals produce a k_z dependence of the d_{xy} band. Calculations in this direction are in progress as well as a detailed study of the Yamaji effect in Sr_2RuO_4.

The Fermi-surface topology obtained here, i.e., two electronlike sheets centered at the Γ point and one holelike sheet centered at the X point, is different from that deduced from ARPES experiments.[10] In these measurements the Fermi surface seems to be composed by two hole-like sheets and one electronlike sheet. Moreover, in both cases the electron count

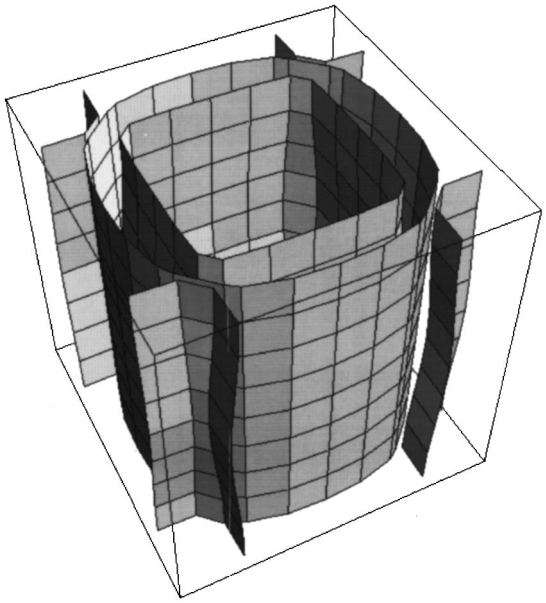

FIG. 3. Calculated Fermi surfaces in the Brillouin zone. Perspective view of the hole and electron sheets of the Fermi surface derived from the hybridized Ru d_{xz}, d_{yz}, and d_{xy} bands in the Brillouin zone. The largest electronlike Fermi surface corresponds to the hybridized d d_{xy} band. The center of this Brillouin zone is the Γ point.

is the same. According to the results reported in,[25,3] the discrepancy between the Fermi surface topology observed in the photoemission experiments and in LDA calculations and dHvA measurements, as well as in the results of this paper, could be related to the fact that dHvA and band structure computations yield the bulk electronic structure of Sr_2RuO_4 while ARPES results reflect the surface structure. It is also worth noticing that ARPES Fermi surfaces would yield dHvA frequencies of 3, 8.7, and 10.8 kT (Ref. 26) instead of measured values of 3.05, 12.7, and 18.5 kT, each of which number is accurate to 1%. We want to stress that the dHvA identification of one small hole pocket and two electron pockets is also consistent with the negative sign of the Hall coefficient at low temperatures.

The values of the average Fermi wave vectors of the three sheets and the total density of states (DOS) at the Fermi energy are summarized in Table II where the experimental and LDA averaged Fermi wave vectors are also reported. From an inspection of this table we can observe a quite good agreement between experimental results and the data obtained in the present paper.

TABLE II. Fermi parameters for the three bands. In the first column is reported the MO; column 2 contains the Fermi wave vector (k_F) here calculated; in columns 3 and 4 are reported the experimental and LDA k_F. Column 5 refers to the density of states at E_F.

Band	k_F Å^{-1}	k_F (LDA) Å^{-1}	k_F (expt.) Å^{-1}	$\rho(E_F)$ states/Ry
E_1	0.766	0.732	0.75	30.8
E_2	0.312	0.319	0.302	3.6
E_3	0.618	0.638	0.621	22.6

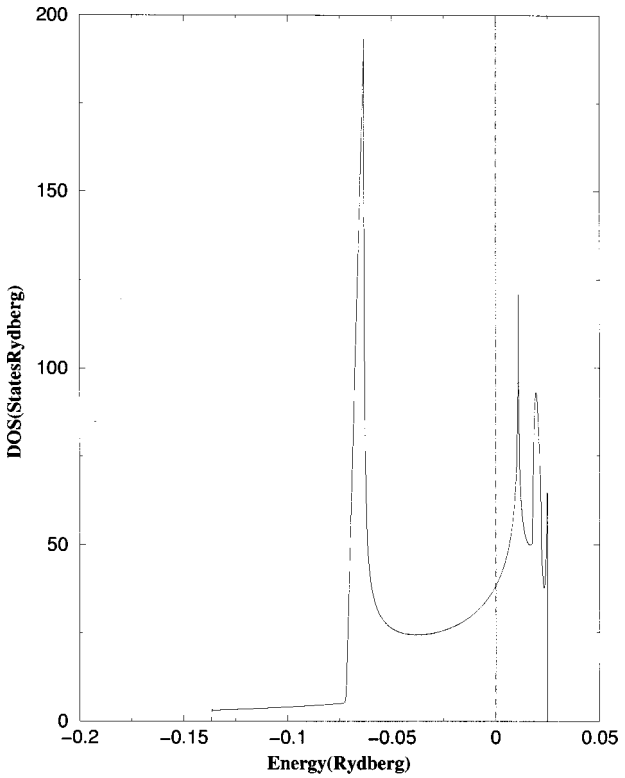

FIG. 4. Total density of states. The Fermi level is denoted by the vertical dashed line.

The total density of states is plotted in Fig. 4. At first sight, one can observe three peaks well separated which are due to Van Hove singularities (VHS's) present in each band that are related to the almost dispersionless character of the bands along the k_z direction. The position of E_F (dot line) falls on the low-energy side of the sharp peak that occurs approximately at 0.1 eV above E_F and is related to the first VHS. This VHS is due to the change in Fermi surface topology that happens rigidly shifting the lower of the two bands crossing E_F along the long Γ-Z direction, in a way that the maximum gets close to the singularity. It is worth pointing out that the realization, if it is possible, of removing about 0.1 O(2) atoms per cell would position the E_F at this VHS, giving insight on the effect on superconductivity of the enhancement of the DOS at E_F. The upper of the two bands leads to a second VHS close to the band edge at 0.28 eV approximately above E_F, while the holelike band presents a sharp peak close to the bottom of the DOS at approximately 1 eV below E_F. The value of the density of states at the Fermi energy is $\rho(E_F)=57$ states/Ry, which is in good agreement with the LDA estimate of 56.2 states/Ry.[6] The present $\rho(E_F)$ value gives a temperature linear coefficient in the specific heat of 9.88 mJ/K^2 mol and Pauli paramagnetic susceptibility of 1.35×10^{-4} emu/mol which are smaller with respect to the observed results on the normal state properties, namely, $\gamma_{\rm exp}=39$ mJ/K^2 mol and $\chi_{\rm exp}=9.7\times10^{-4}$ emu/mol.[1]

The explicit knowledge of the energy spectrum gets also possible the calculation of several transport properties. As an application, here we will determine the temperature dependence of the Hall coefficient R_H.

As referred to in the Introduction, R_H has a complicated

temperature dependence behavior as might be expected for a material with electronlike and holelike carriers. Assuming that the three sheets of the FS are circular and the mean free path l is isotropic and the same for all the pockets, Mackenzie *et al.*[11] obtained a prediction of $R_H=-0.9\times10^{-10}$ m^3/C that compares well with the measured value of -1.15×10^{-10} m^3/C. This result is improved when l is the same for the two electron pockets but different for the hole one.[11]

We report therein the theoretical calculation of R_H for two types of carriers using the explicit expression for the energy spectrum obtained in the previous section. The in-plane Hall coefficient is given by the following formula:

$$R_H=\frac{\sigma_{xy}}{B\sigma_{xx}^2}.$$

σ_{xy} and σ_{xx} are the in-plane and the x-axis conductivities, respectively, and B is the external applied magnetic field. To compute σ_{xy} and σ_{xx} we use the Jones-Zener expansion of the distribution function $g(k)$ which determines the density current $\vec{J}$ through the formula

$$\vec{J}=\frac{2e}{(2\pi)^3}\int d^3k\vec{v}(k)g(k),$$

where $\vec{v}(k)=1/\hbar\vec{\nabla}\varepsilon(k)$ is the velocity of the particle in k space. Since $g(k)$ is a function of the band energy spectrum we can calculate R_H using the actual energy bands $E_i(k)$.

The x axis and in-plane conductivity for the i band at lowest order can be expressed as follows:

$$\sigma_{xx}^{(i)}=\frac{2e}{(2\pi)^3\hbar^2}\int d^3k\left(-\frac{\partial f}{\partial E_i}\right)\tau_i\left(\frac{\partial E_i}{\partial k_x}\right)^2$$

and

$$\sigma_{xy}^{(i)}=-\frac{2e^3B}{(2\pi)^3\hbar^4}\int d^3k\left(-\frac{\partial f}{\partial E_i}\right)\tau_i\left(\frac{\partial E_i}{\partial k_x}\right)$$

$$\times\left[\frac{\partial E_i}{\partial k_y}\frac{\partial}{\partial k_x}\left(\tau_i\frac{\partial E_i}{\partial k_y}\right)-\frac{\partial E_i}{\partial k_x}\frac{\partial}{\partial k_y}\left(\tau_i\frac{\partial E_i}{\partial k_y}\right)\right].$$

Here f is the Fermi function and τ_i is the relaxation time related to the band $E_i(k)$. To calculate explicitly R_H we suppose that τ_i is isotropic, i.e., k independent and varies as T^2 for each band.[27] This assumption is based on the hypothesis of a scattering dominated by the electron-electron and hole-hole interaction and this in turn implies that the resistivity varies as T^2, as experimentally observed at low temperatures.[12,13] Therefore, it is natural to assume for each band

$$\tau_i=A_i+B_iT^2\quad(i=1,2,3),$$

where A_i and B_i are ad hoc constants. Generalizing the expression of R_H for a multiband system we have[28]

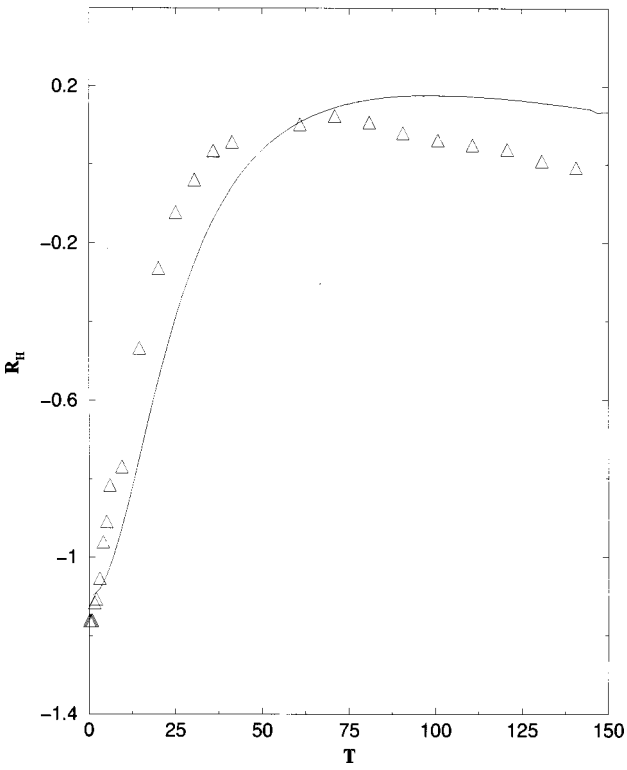

FIG. 5. Temperature dependence of the in-plane Hall coefficient R_H. R_H is measured in 10^{-10} m^3/C. The triangles denote the experimental data taken from Ref. 10.

$$R_H=\frac{\sum_i\sigma_{xy}^{(i)}}{B\sum_i(\sigma_{xx}^{(i)})^2}.$$

The low-temperature behavior of R_H is plotted in Fig. 5. The curve has been obtained using for the electronlike bands the same τ, with $A=1.13$ and $B=0.0023$, while $A=1$ and $B=0.0016$ have been used for the holelike band. In the same figure the experimental data reported in (Ref. 11) are represented by triangles. We can see that we reproduce the sign change from negative to positive value at low temperatures but the actual variation of R_H with temperature is more complex. Indeed, our results reproduce with quite good accuracy the trend of experimental data only for temperatures less than 40 K. This discrepancy may be related to the assumption made for the relaxation rates. Both the in-plane ρ_{ab} and out of plane ρ_c resistivity vary as T^2, to high accuracy, only below 25 K. Above this temperature, ρ_{ab} raises monotonically and it can be modeled well with a weighted sum of T and T^2 contributions, with a sharp T component, whereas ρ_c shows a pronounced peak at about 130 K.[12,13] This behavior results in a change of the temperature dependence of the scattering amplitude probability implying a deviation from a T^2 power law for τ.

IV. CONCLUSIONS

The electronic energy band structure of Sr_2RuO_4 has been calculated by using a simple combined EHT–tight-binding method. Our calculations reproduce with good accuracy

LDA results, showing almost dispersionless Fermi surfaces along k_z direction and thus supporting the quasi two dimensional nature of Sr_2RuO_4.

We have derived an appropriate tight-binding Hamiltonian, as well as analytical expressions for energy bands and for the constant-energy contour near the Fermi surface. We point out that the analytical formula for energy bands of electrons around the Fermi level here presented can be readily used to analyze physical quantities in which the topology of the Fermi surface is important as well as the possibility of superconducting instability within the standard broken-symmetry Hartree-Fock scheme. In this respect, we have computed the temperature dependence of the Hall coefficient assuming that the main contribution to scattering of carriers is electron-electron or hole-hole interaction and varies with a T^2 power law. This model can reproduce the sign changes of R_H but not the behavior above 70 K, where the Hall coefficient starts to decrease. A more sophisticated model including the temperature dependence of the chemical potential as well as the k dependence of τ and a different temperature law for the relaxation rate needs to explain the temperature behavior of R_H and is currently being developed. Calculations in this direction are in progress and will be presented in a forthcoming publication.

ACKNOWLEDGMENTS

It is a pleasure to thank Professor A. Mackenzie, Dr. T. Xiang, Professor A. Oleś, and Professor P. Horsch for helpful discussions and comments.

APPENDIX

In the following for completeness we report the expression of hopping parameters introduced in Sec. II:

$$t_{1i}(k) = -2t_{1i}\sin(k_i/2 \quad (i=x,y), \tag{A1}$$

$$t_2(k) = -4t_2\sin(k_x/2)\sin(k_y/2),$$

$$a_k = -4t_3\cos(k_x/2)\cos(k_y/2),$$

$$b_k = 4t_4\cos(k_x/2)\sin(\alpha k_z/2),$$

$$c_k = 4t_4\cos(k_y/2)\sin(\alpha k_z/2),$$

$$e_k = 2t_5\sin(k_x/2),$$

$$f_k = 2t_5\sin(k_y/2),$$

$$g_k = 2t_6\sin(\alpha k_z/2).$$

Using these quantities the E_3 band reads as follows:

$$E_3 = \frac{[\varepsilon_{xy}((\varepsilon_p-\mu)^2 - t_2^2) + \mu t_{1x}{}^2 + 2t_2 t_{1x} t_{1y} + \mu t_{1y}^2 - \varepsilon_p(t_{1x}^2 + t_{1y}^2)]}{[(\varepsilon_p-\mu)^2 - t_2^2]}.$$

By mean of Eqs. (A1) and the definitions below one can write the hybridized $E_{1,2}$ bands in the following way:

$$E_1 = \tfrac{1}{2}[a_{11} + a_{22} + \sqrt{(a_{11}-a_{22})^2 + 4|a_{12}|^2}],$$

$$E_2 = \tfrac{1}{2}[a_{11} + a_{22} - \sqrt{(a_{11}-a_{22})^2 + 4|a_{12}|^2}],$$

where

$$a_{11} = \frac{N_1}{D},$$

$$a_{22} = \frac{N_2}{D},$$

$$a_{12} = a_{21}^* = \frac{N_3}{D},$$

with

$$\begin{aligned}
N_1 &= b_k^2\varepsilon_d(c_k+\varepsilon_p-\mu)(c_k-\varepsilon_p+\mu) + (\varepsilon_p-\mu) \\
&\quad \times\{a_k^2(-\varepsilon_d\varepsilon_p + g_k^2) \\
&\quad + (c_k-\varepsilon_p)(c_k+\varepsilon_p)(e_k^2 - \varepsilon_d\varepsilon_p + g_k^2) \\
&\quad + [2e_k^2\varepsilon_p + \varepsilon_d(a_k^2 + c_k^2 - 3\varepsilon_p^2) + 2\varepsilon_p g_k^2]\mu \\
&\quad - (e_k^2 - 3\varepsilon_d\varepsilon_p + g_k^2)\mu^2 - \varepsilon_d\mu^3\}, \\
N_2 &= b_k^2(c_k^2\varepsilon_d - [f_k^2 - g_k^2 + \varepsilon_d(\varepsilon_p-\mu)](\varepsilon_p-\mu)) \\
&\quad - \{a_k^2(-g_k^2 + \varepsilon_d(\varepsilon_p-\mu)) \\
&\quad + [c_k^2\varepsilon_d - (f_k^2 - g_k^2 + \varepsilon_d(\varepsilon_p-\mu)](\varepsilon_p-\mu)\}(\varepsilon_p-\mu), \\
N_3 &= a_k(ib_k g_k + e_k(\varepsilon_p-\mu))(\varepsilon_p f_k - ic_k g_k - f_k\mu), \\
D &= [b_k(-c_k^2 + (\varepsilon_p-\mu)^2) \\
&\quad + (\varepsilon_p-\mu)^2(-a_k^2 - c_k^2 + \varepsilon_p^2 - 2\varepsilon_p\mu + \mu^2)].
\end{aligned}$$

[1] Y. Maeno, H. Hashimoto, K. Yoshida, S. Nishizaki, T. Fujita, J. G. Bednorz, and F. Lichtenberg, Nature (London) **372**, 532 (1994).

[2] D. F. Agterberg, T. M. Rice, and M. Sigrist, Phys. Rev. Lett. **78**, 3374 (1997).

[3] I. I. Mazin and D. Singh, Phys. Rev. Lett. **79**, 733 (1997).

[4] A. P. Mackenzie, R. K. Haselwimmer, A. W. Tyler, G. G. Lonzarich, Y. Mori, S. Nishizaki, and Y. Maeno, Phys. Rev. Lett. **80**, 161 (1998).

[5] T. Oguchi, Phys. Rev. B **51**, 1385 (1995).

[6] D. J. Singh, Phys. Rev. B **52**, 1358 (1995).
[7] G. J. McMullan, M. P. Ray, and R. J. Needs, Physica B **223-224**, 529 (1996).
[8] A. P. Mackenzie, S. R. Julian, A. J. Diver, G. J. McMullan, M. P. Ray, G. G. Lonzarich, Y. Maeno, S. Nishizaki, and T. Fujita, Phys. Rev. Lett. **76**, 3786 (1996).
[9] Y. Yoshida, R. Settai, Y. Onuki, H. Takei, K. Betsuyaku, and H. Harima, J. Phys. Soc. Jpn. **67**, 1677 (1998).
[10] T. Tokoya, A. Chainani, T. Takahashi, H. Katayama-Yoshida, M. Kasai, and Y. Tokura, Phys. Rev. Lett. **76**, 3009 (1996); D. H. Lu, M. Schmidt, T. R. Cummins, S. Schuppler, F. Lichtenberg, and J. G. Bednorz, *ibid.* **76**, 4845 (1996); T. Tokoya, A. Chainani, T. Takahashi, H. Ding, J. C. Campuzano, H. Katayama-Yoshida, M. Kasai, and Y. Tokura, Phys. Rev. B **54**, 13 311 (1996).
[11] A. P. Mackenzie, N. E. Hussey, A. J. Diver, S. R. Julian, Y. Maeno, S. Nishizaki, and T. Fujita, Phys. Rev. B **54**, 7425 (1996).
[12] F. Lichtenberg, A. Catana, J. Mannhart, and D. G. Schlom, Appl. Phys. Lett. **60**, 1138 (1992).
[13] N. E. Hussey, A. P. Mackenzie, J. R. Cooper, Y. Maeno, S. Nishizaki, and T. Fujita, Phys. Rev. B **57**, 5505 (1998).
[14] H. Yoshino, K. Murata, N. Shirakawa, Y. Nishihara, Y. Maeno, and T. Fujita, J. Phys. Soc. Jpn. **65**, 1548 (1996).
[15] A. Yamanaka, N. Asayama, M. Sasada, K. Inoue, M. Udagawa, S. Nishizaki, Y. Maeno, and T. Fujita, Physica C **263**, 516 (1996).
[16] I. H. Inoue, Y. Aiura, Y. Nishihara, Y. Haruyama, S. Nishizaki, Y. Maeno, T. Fujita, J. G. Bednorz, and F. Lichtenberg, Physica B **223-224**, 516 (1996).
[17] P. W. Anderson, in *The Theory of Superconductivity in the High T_c Cuprates*, Princeton Series in Physics (Princeton University Press, Princeton, NJ, 1997), Chap. 1; P.W. Anderson, Philos. Trans. R. Soc. London, Ser. A **334**, 473 (1989); O. K. Andersen, O. Jepsen, A. I. Liechetenstein, and I. I. Mazin, Phys. Rev. B **49**, 4145 (1994).
[18] M. Cuoco, C. Noce, and A. Romano, Phys. Rev. B **57**, 11 989 (1998).
[19] C. Noce and T. Xiang, Physica C **282-287**, 1713 (1997).
[20] T. Vogt and D. J. Buttrey, Phys. Rev. B **52**, 9843 (1995).
[21] R. Hoffmann, J. Chem. Phys. **39**, 1937 (1963).
[22] Y. T. Wong, A. W. E. Chan, and R. Hoffmann, Int. J. Mod. Phys. B **4**, 677 (1990).
[23] M. Schmidt, T. R. Cummins, M. Bürk, D. H. Lu, N. Nücker, S. Schuppler, and F. Lichtenberg, Phys. Rev. B **53**, 14 761 (1996).
[24] O. K. Andersen, A. I. Liechtenstein, O. Jepsen, and F. Paulsen, J. Phys. Chem. Solids **56**, 1573 (1995).
[25] A. P. Mackenzie, S. R. Julian, G. G. Lonzarich, Y. Maeno, and T. Fujita, Phys. Rev. Lett. **78**, 2271 (1997).
[26] A. P. Mackenzie (private communication).
[27] N. Shirakawa, K. Murata, Y. Nishihara, S. Nishizaki, Y. Maeno, T. Fujita, J. G. Bednorz, F. Lichtenberg, and N. Hamada, J. Phys. Soc. Jpn. **64**, 1072 (1995).
[28] J. M. Ziman, *Principle of the Theory of Solids* (Cambridge University Press, Cambridge, 1979).